Claim-Bounded Diagnostics for a Localized Early-Time A10 Cosmology Branch: Reduced-Surrogate Evidence, 137-Stability Gating, and Optional Growth-Suppression Tests

Keiji Yoshimura
Independent Researcher

April 2026; revised May 2026

Abstract

This manuscript reframes the A10 cosmology program as a claim-bounded diagnostic study of one localized early-time branch relevant to the Hubble-tension problem. The branch centers on an energy-transfer episode near $z \approx 5000$, first posed phenomenologically and later implemented as a conversion from a quasi-vacuum parent component Y to a stiff daughter component X in a perturbative treatment based on CLASS. The reported diagnostic evidence suggests that a sufficiently early and localized transfer can reduce the sound horizon while producing smaller acoustic-phase distortions than a simple constant-$\Delta N_{\rm eff}$ benchmark within the tested setup. The manuscript then examines a spectral-Horndeski stability window near $\chi \approx 137$ as a possible field-space trigger for selective activation. A root-geometric analysis is retained only as a conceptual model of selectivity, not as a literal cosmological derivation. Within the reported Markov Chain Monte Carlo analysis of the gated branch, the preferred region reaches a high-H_0 candidate regime near $H_0 \approx 73\,\mathrm{km\,s^{-1}\,Mpc^{-1}}$ together with a self-adjusted dark matter density $\omega_{\rm cdm} \approx 0.1087$. As a separate optional extension, a late-time momentum-drag sector is summarized as a limited growth-suppression test that introduces a trade-off with CMB lensing consistency. The intended contribution is not a final resolution of the Hubble tension, not a universal model-selection claim, and not an observational discovery. It is a reduced-surrogate and diagnostic framework for organizing one candidate mechanism, its internal evidence hierarchy, and the next validation steps required before stronger cosmological claims would be justified.

Reader Guidance and Claim Boundary

This revised version is written to make the evidential status of the manuscript explicit before the technical construction begins. The paper should be read under the following boundaries.

- **Allowed interpretation.** The manuscript describes a reduced, claim-bounded diagnostic branch in which localized early-time energy transfer, field-space gating, and optional late-time drag are organized into a testable modeling sequence.
- **Not claimed.** The manuscript does not establish a final solution to the Hubble tension, does not prove that A10 is preferred over all alternatives, and does not claim that 137 is a universal cosmological constant.

- **Evidence status.** The figures, posterior summaries, and shuffle diagnostics are treated as branch-level numerical evidence within the reported implementation, not as independent observational validation.
- **Role of auxiliary sectors.** The root-geometric material is a selectivity analogy, and the late-time drag model is an optional companion test; neither is part of the minimal early-time claim.
- **Next validation need.** Stronger claims require independent reproduction, systematic likelihood comparison, robustness testing under alternative closures, and expert review against current cosmological data pipelines.

1 Introduction

The Hubble tension remains one of the central anomalies of precision cosmology. In the standard flat ΛCDM model, the CMB-inferred value of the Hubble constant from *Planck* differs significantly from direct late-universe determinations such as SH0ES [1, 2]. A broad class of proposed resolutions attempts to raise the inferred H_0 by reducing the sound horizon prior to recombination, but many such constructions face a familiar difficulty: the same early-time modification that boosts the expansion rate can also induce acoustic-phase shifts, damping-tail distortions, or late-time inconsistencies that limit the allowed parameter space [3, 4, 5].

The A10 program explores a particular branch of this problem. Its core hypothesis is that an early-universe energy-transfer episode, if sufficiently localized and placed earlier than the standard $z \sim 3000$ early-dark-energy window, can reduce the sound horizon while leaving recombination-era observables comparatively gentle. In the original phenomenological picture, this transfer was specified directly as a redshift-localized kernel near $z \approx 5000$. In the later dynamical picture, the same transfer is reinterpreted as a field-space event that activates only inside a stability-protected window near $\chi \approx 137$.

The purpose of the present manuscript is not simply to concatenate several related notes or to present a finished cosmological solution. Rather, it is to articulate their common logic in a more disciplined hierarchy. The primary claim of the paper concerns the *localized early-time A10 branch* and a proposed *137-gated dynamical organization* within the reported reduced implementation. A secondary claim is that the spectral-Horndeski sector provides a plausible stability-based trigger for selectivity in field space. A further conceptual support is supplied by a root-geometric leakage argument, whose role is interpretive rather than literal. Finally, an optional late-time momentum-drag sector is discussed as a companion extension for mild growth suppression, not as a foundational ingredient of the early-time H_0 mechanism itself.

The paper is therefore organized around the following questions: (i) can a localized transfer near $z \approx 5000$ be organized as a controlled candidate branch for the early-time H_0 problem without introducing the large phase shifts characteristic of a simple constant-$\Delta N_{\rm eff}$ benchmark; (ii) can that transfer be reinterpreted as a dynamically protected event in field space; and (iii) what is the appropriate scope of the resulting claim? Our answer is deliberately restrained. We argue only that the integrated A10 framework defines a candidate model class with reported numerical support for a high-H_0 branch inside the tested setting; it is not yet a definitive observational selection over competing scenarios.

2 Phenomenological Origin of the A10 Branch

2.1 A localized transfer centered near $z \approx 5000$

The phenomenological starting point of the A10 branch is a sharply localized energy-transfer kernel centered near $z \approx 5000$, illustrated in Fig. 1. In the original formulation, the transfer rate was written as

$$\epsilon(a) = \gamma_* \exp\left[-\frac{\ln^2(a/a_*)}{2\sigma_*^2}\right], \tag{1}$$

where a_* denotes the peak transfer epoch and σ_* controls the width in $\ln a$. The basic intent is to modify the early expansion history in a compact window that is well separated from the visibility peak.

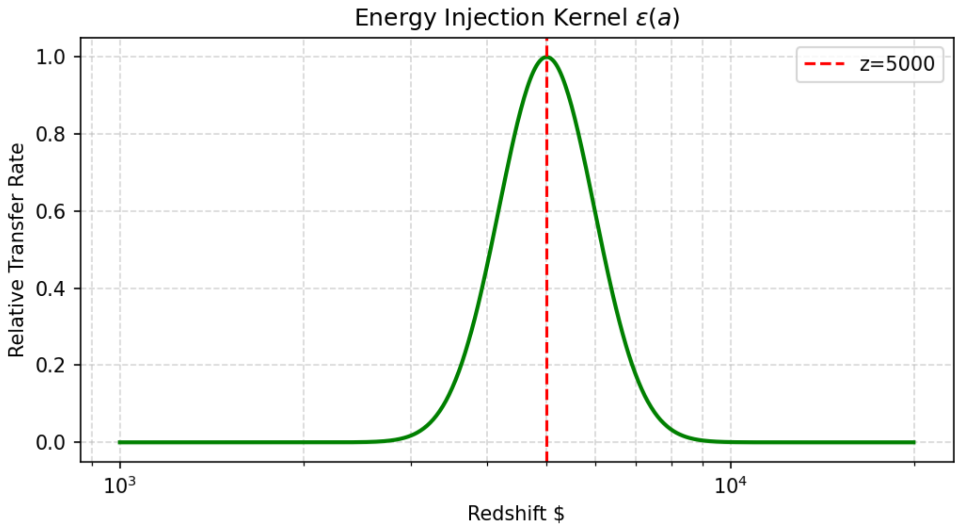

Figure 1: Localized A10 transfer kernel centered near $z \approx 5000$. The function identifies the early-time window in which the expansion history is modified before recombination while remaining sufficiently separated from the visibility peak.

A later and more concrete implementation of this idea treats the transfer as a conversion from a quasi-vacuum parent fluid Y to a stiff daughter fluid X:

$$H^2 = \frac{8\pi G}{3}\left(\rho_{\rm std} + \rho_Y + \rho_X\right), \tag{2}$$

$$\frac{d\rho_Y}{d\ln a} = -\epsilon(a)\rho_Y, \tag{3}$$

$$\frac{d\rho_X}{d\ln a} = -3(1 + w_X)\rho_X + \epsilon(a)\rho_Y, \tag{4}$$

with $w_Y \simeq -1$ and $w_X = 1$. Earlier notes also explored a phenomenological dark-radiation conversion picture, but in the present integrated manuscript the quasi-vacuum-to-stiff realization is treated as the principal dynamical implementation. The full perturbation system was studied within CLASS [6, 7].

2.2 Why the transfer is earlier than standard EDE

The main phenomenological motivation for placing the transfer near $z \approx 5000$ rather than the more familiar $z \sim 3000$ EDE window is straightforward. The aim is not merely to raise the early expansion rate, but to do so while reducing direct interference with recombination-era microphysics. A transfer that occurs sufficiently early can shrink the sound horizon but leave the observed acoustic pattern more controlled than a simpler constant-$\Delta N_{\rm eff}$ deformation [3, 4, 5].

This point is sharpened by the contrast between a background-only implementation and a full perturbative realization. Figure 2 shows that a background-only modification (labeled A9 in the author's sequence) does not by itself reproduce the observed acoustic structure, whereas the full A10 perturbative realization does substantially better. The distinction is crucial: the A10 branch is not simply a rescaled background history, but a perturbatively self-consistent model class.

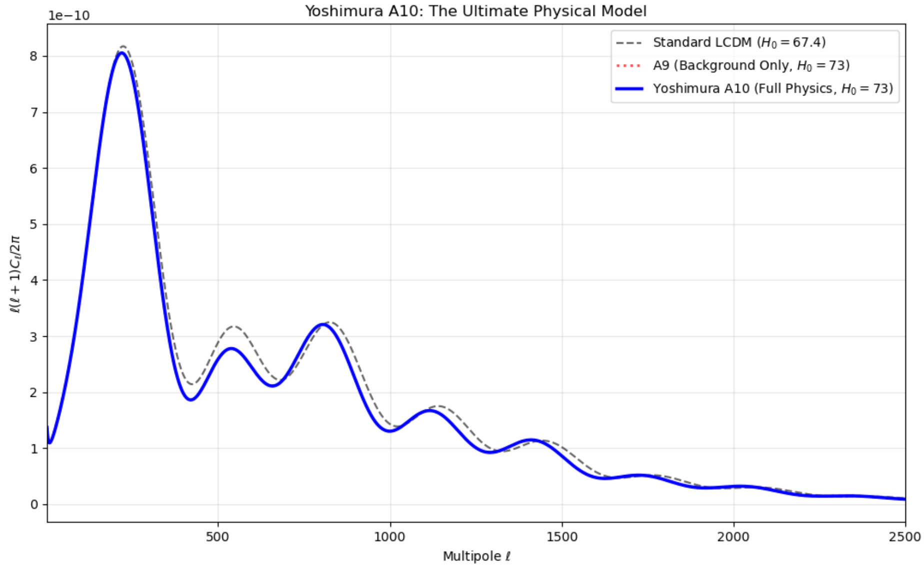

Figure 2: Background-only versus full-physics implementation of the A10 scenario. The background-only branch modifies the expansion history but does not restore the acoustic structure, whereas the full A10 realization evolves the coupled perturbations self-consistently and remains substantially closer to the standard CMB pattern.

3 Observable Signatures: TT, EE, TE, and BAO

3.1 Direct TT comparison with standard ΛCDM

Figure 3 shows a direct comparison between the A10 branch and the standard ΛCDM TT spectrum. The point of this comparison is not to claim exact indistinguishability. Rather, it is to show that the A10 branch can alter the early-time sound horizon while keeping the detailed acoustic residual structure comparatively controlled.

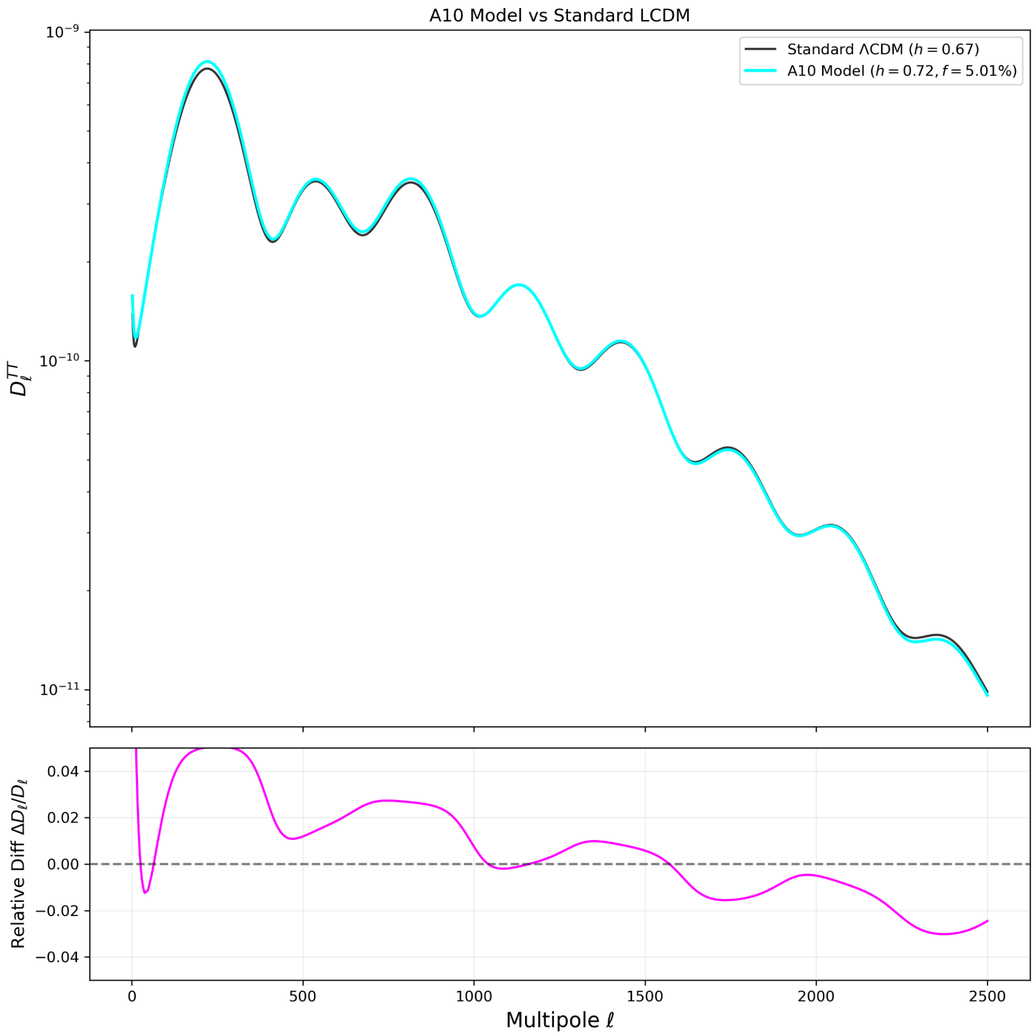

Figure 3: Direct TT comparison between the A10 branch and standard ΛCDM. The residual panel shows that the A10 branch modifies the inferred sound horizon while leaving the acoustic pattern comparatively controlled rather than grossly reshaped.

3.2 A10 versus a simple dark-radiation benchmark

The more informative comparison is not with ΛCDM alone but with a simple benchmark that increases the early radiation content. Figure 4 compares the A10 branch with a constant-$\Delta N_{\rm eff}$-type dark-radiation reference. The distinctive feature is not an absence of any spectral response; it is the relative suppression of the broad oscillatory phase shift that typically accompanies the simpler benchmark. This is the key observational motive for treating the A10 branch as a separate phenomenological direction.

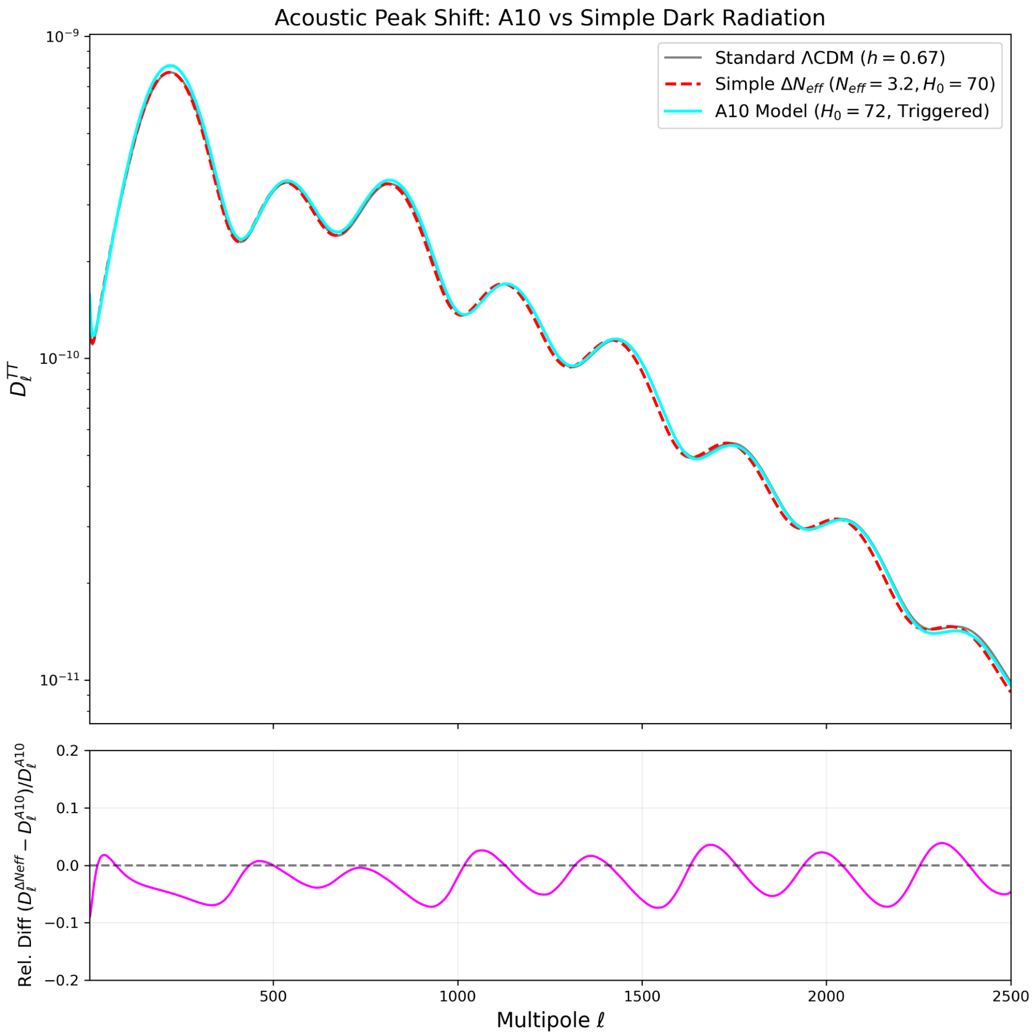

Figure 4: TT comparison between standard ΛCDM, a simple dark-radiation benchmark, and the A10 branch. The central diagnostic observation is that the tested A10 branch raises H_0 in the reported setup while suppressing the larger acoustic-phase distortion characteristic of the simpler benchmark extension.

3.3 Polarization-level tests

The A10 branch is not expected to be completely hidden from high-ℓ polarization. Figures 5(a) and 5(b) show that although the TT phase shift is comparatively controlled, EE and TE still retain nontrivial structure. This is an important point for scope: the model is designed to be *gentler*, not invisible.

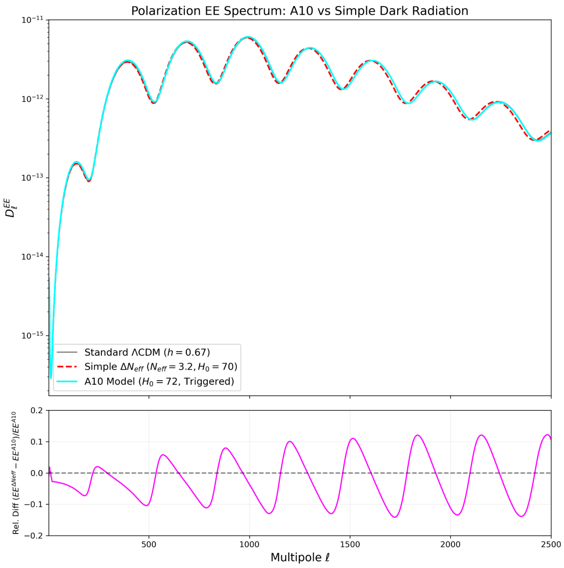

(a) EE comparison.

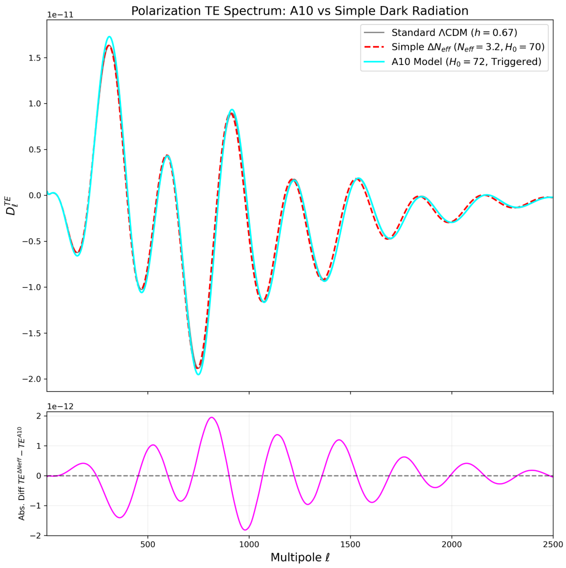

(b) TE comparison.

Figure 5: Polarization-level comparison between the A10 branch and a simple dark-radiation benchmark. The A10 construction remains observationally testable in EE and TE even when the dominant TT phase shift is comparatively suppressed.

3.4 Late-time distance check with BAO

A model that alleviates the early-time H_0 tension but fails catastrophically in late-time distances does not constitute a meaningful improvement. Figure 6 therefore compares the BAO observable D_M/r_d with BOSS DR12 measurements [8]. Within the reported analysis, the A10 branch remains reasonably controlled at the late-time distance level while targeting a higher-H_0 candidate regime. The proper claim here is modest: within the present parameterization, the branch appears to trade a severe early-time discrepancy for a substantially milder late-time-distance residual rather than removing all tension.

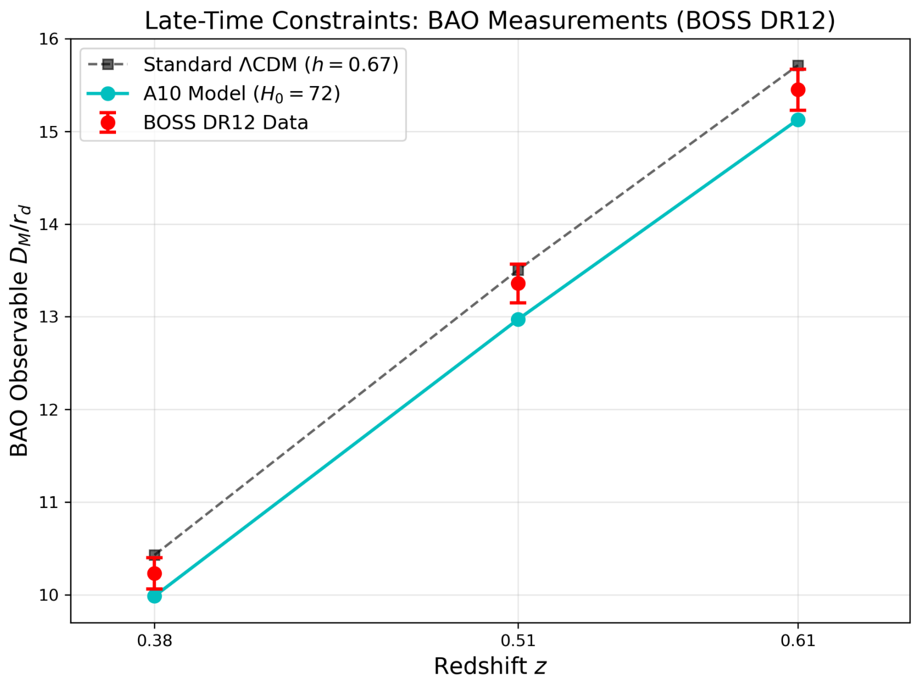

Figure 6: BAO observable D_M/r_d compared with BOSS DR12 measurements [8]. The A10 branch remains comparatively close to the reported BAO points while targeting a higher-H_0 candidate regime, indicating that late-time distance consistency is degraded only mildly rather than catastrophically within the present model class.

4 A Stability-Protected Trigger Near $\chi \approx 137$

4.1 Spectral-Horndeski setup

The next step is to reinterpret the redshift-localized transfer as a dynamically protected event in field space. To that end, the program introduces a spectral-Horndeski sector with schematic Horndeski functions

$$G_2 = X - V(\chi), \tag{5}$$

$$G_3 = 0, \tag{6}$$

$$G_4 = \frac{1}{2}F(\chi), \tag{7}$$

$$G_5 = 0, \tag{8}$$

with effective Planck mass

$$F(\chi) = 1 + \frac{\xi}{2}(\chi - v_\chi)^2, \tag{9}$$

and spectral contribution

$$V(\chi) = V_{\text{poly}}(\chi) - \mu_{E8}\,\mathcal{L}_{E8}(\chi), \tag{10}$$

where the spectral density is modeled as

$$\mathcal{L}_{E8}(\chi) = \sum_j \frac{\gamma_j}{[s(\chi) - \lambda_j]^2 + \gamma_j^2}. \tag{11}$$

A useful diagnostic of spectral forcing is the sensitivity

$$I(\chi) = |\partial_\chi \mathcal{L}_{E8}|^2 , \tag{12}$$

while ghost stability is monitored through

$$D = \alpha_K + \frac{3}{2}\alpha_B^2. \tag{13}$$

The point of this construction is not to assert a universal metaphysical role for the number 137. It is narrower and more technical: the reported stability margin develops a localized dome near $\chi \approx 137$, while the peak spectral sensitivity occurs earlier, near $\chi_{\mathrm{spec}} \approx 133.6$. This offset suggests a buffered or delayed dynamical response, rather than a direct one-to-one identification between forcing and protection.

4.2 Stability landscape, null test, and ensemble test

Figure 7 shows the dominant stability dome in the spectral-Horndeski sector. The dome is highly localized relative to the null baseline, which motivates the interpretation of a field-space protection window.

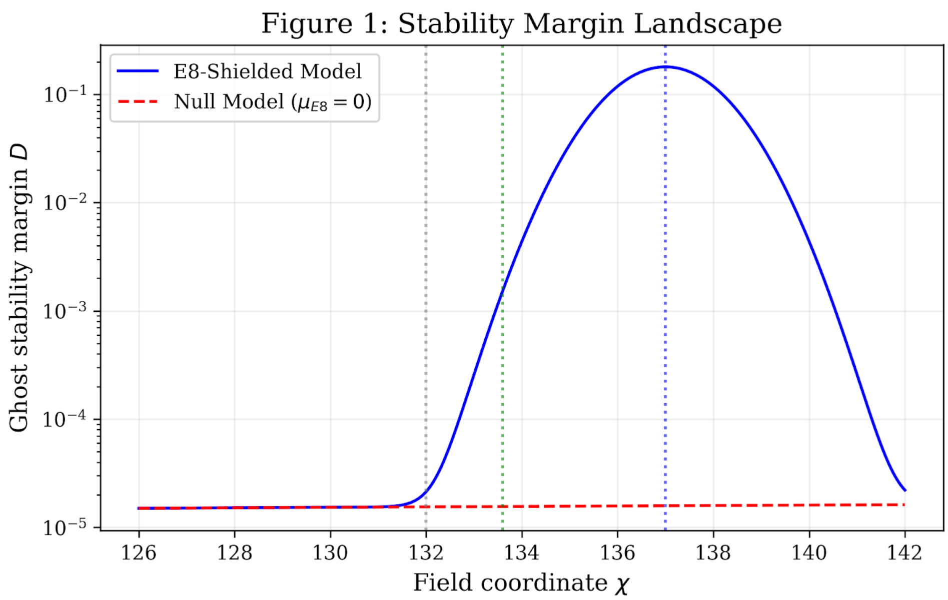

Figure 7: Stability-margin landscape in the spectral-Horndeski sector. The dominant protection dome appears near $\chi \approx 137$ relative to the null baseline, motivating the interpretation of a stability-protected activation window in field space.

The null and shuffle diagnostics matter because a single localized curve can otherwise be dismissed as fit tuning. Figure 8 summarizes the ensemble-level comparison: the coherent realization is an outlier both in peak stability margin and in its localization near $\chi \approx 137$. This does not prove uniqueness in any stronger sense, but it does support the narrower claim that the reported dome is not behaving like a generic shuffled surrogate.

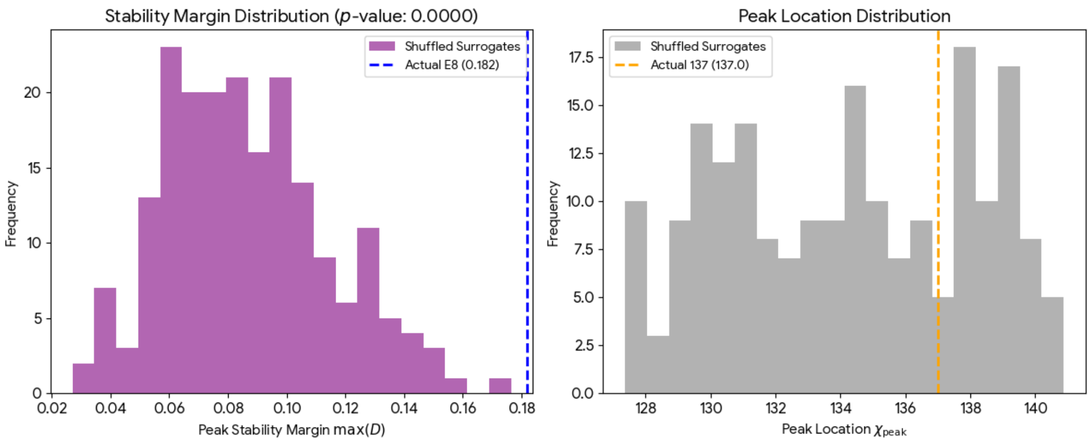

Figure 8: Ensemble-level summary of shuffle diagnostics for the spectral-Horndeski sector. The coherent realization lies in the extreme tail of the shuffled peak-height distribution and remains localized near $\chi \approx 137$, supporting the interpretation of a non-generic stability dome.

4.3 Information-geometric reading

Figure 9 provides a compact visualization of the offset between the spectral-information surge and the stability peak. In the integrated reading, the scalar first encounters a region of maximal forcing and only later enters the most protected part of field space. This is why the language of *stability buffering* or *stability inertia* is more appropriate than any stronger claim of exact coincidence.

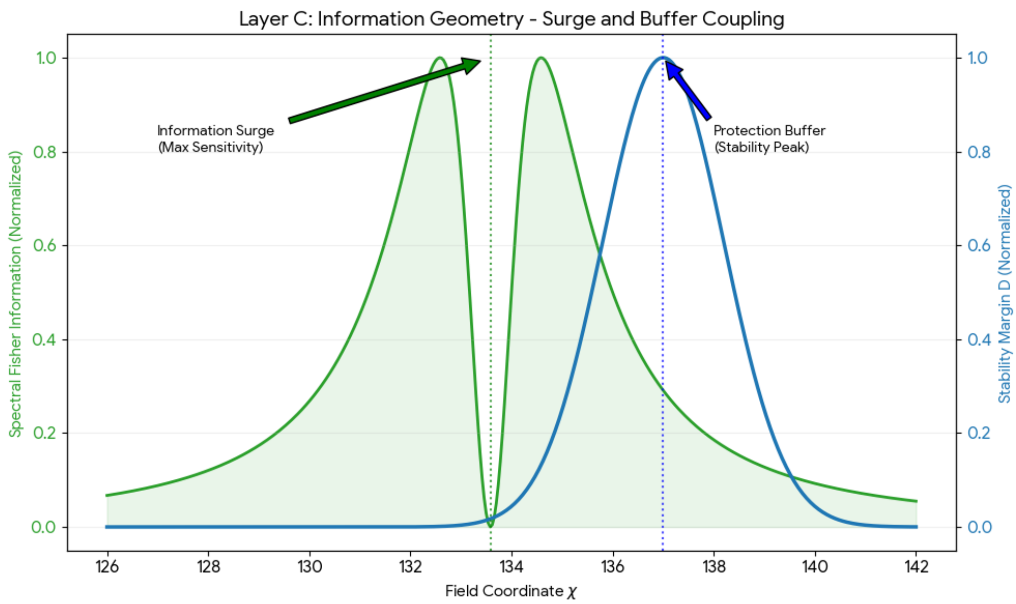

Figure 9: Information-geometric interpretation of the spectral-stability hierarchy. The normalized spectral-information surge occurs upstream of the dominant stability peak, consistent with a buffered transition from forcing to protection.

5 A 137-Gated Candidate Branch

5.1 From redshift localization to field-space activation

The conceptual move that defines the integrated model is to promote the original phenomenological transfer to a field-dependent gate,

$$g(\chi) = g_0 \exp\left[-\frac{(\chi - \chi_g)^2}{2\sigma_g^2}\right], \qquad \chi_g \approx 137. \tag{14}$$

In words, the transfer is activated only when the scalar field enters the stability-protected window identified by the spectral-Horndeski analysis. The injection epoch is therefore no longer a purely external choice in redshift space, but is synchronized with a preferred region of field space.

Figure 10 summarizes the resulting logic. The stability dome activates the gate; the gate triggers a rapid transfer into a stiff-fluid component; the transfer boosts the early expansion rate near $z \approx 5000$; and the target observable consequence is a reduced sound horizon with controlled impact on the CMB acoustic structure.

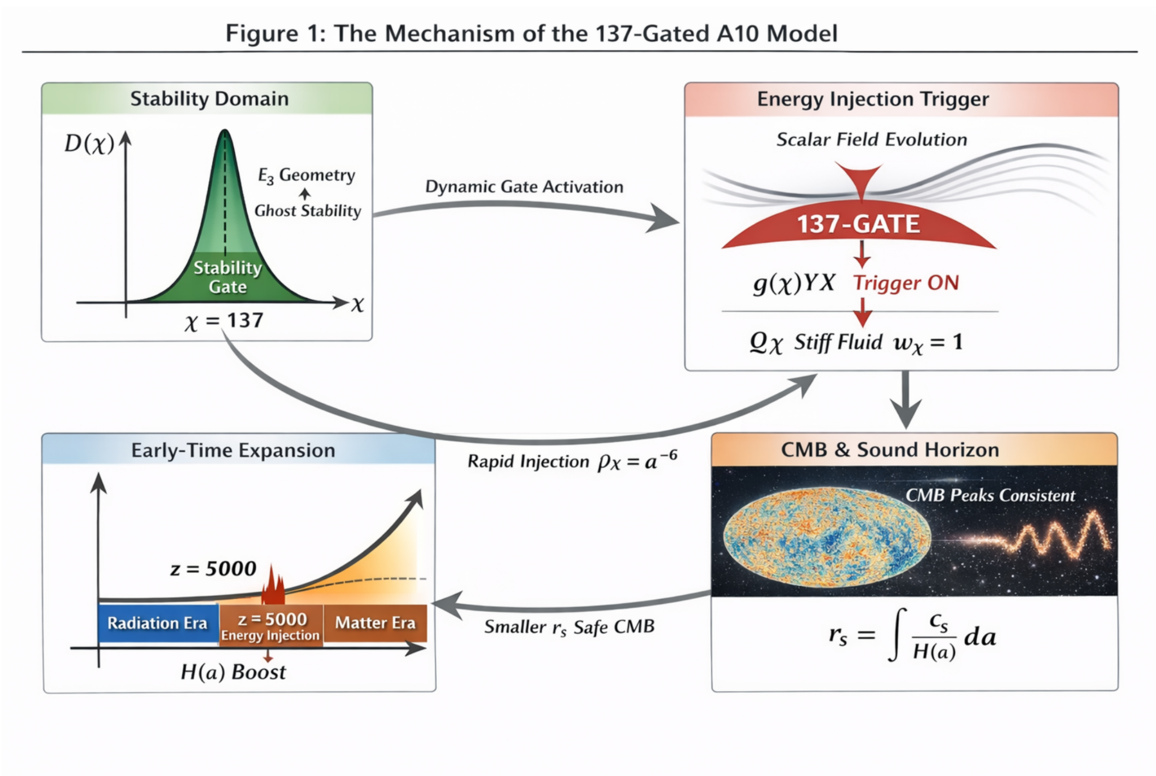

Figure 10: Schematic mechanism of the 137-gated A10 model. The transfer is localized not only in redshift space but also in field space: the scalar must enter a stability-protected window before the early-time energy injection is activated.

5.2 Reported parameter-space behavior

The reported Markov Chain Monte Carlo analysis of the gated branch reaches a high-H_0 region near

$$H_0 \approx 73\,\mathrm{km\,s^{-1}\,Mpc^{-1}}, \tag{15}$$

while the cold-dark-matter density shifts to

$$\omega_{\rm cdm} \approx 0.10873 \pm 0.00033. \tag{16}$$

The important point is that the dark sector does not remain passive while the gate activates. Instead, the preferred region reflects a coupled adjustment: the early-time expansion boost and the later-time matter budget co-vary within the fitted branch.

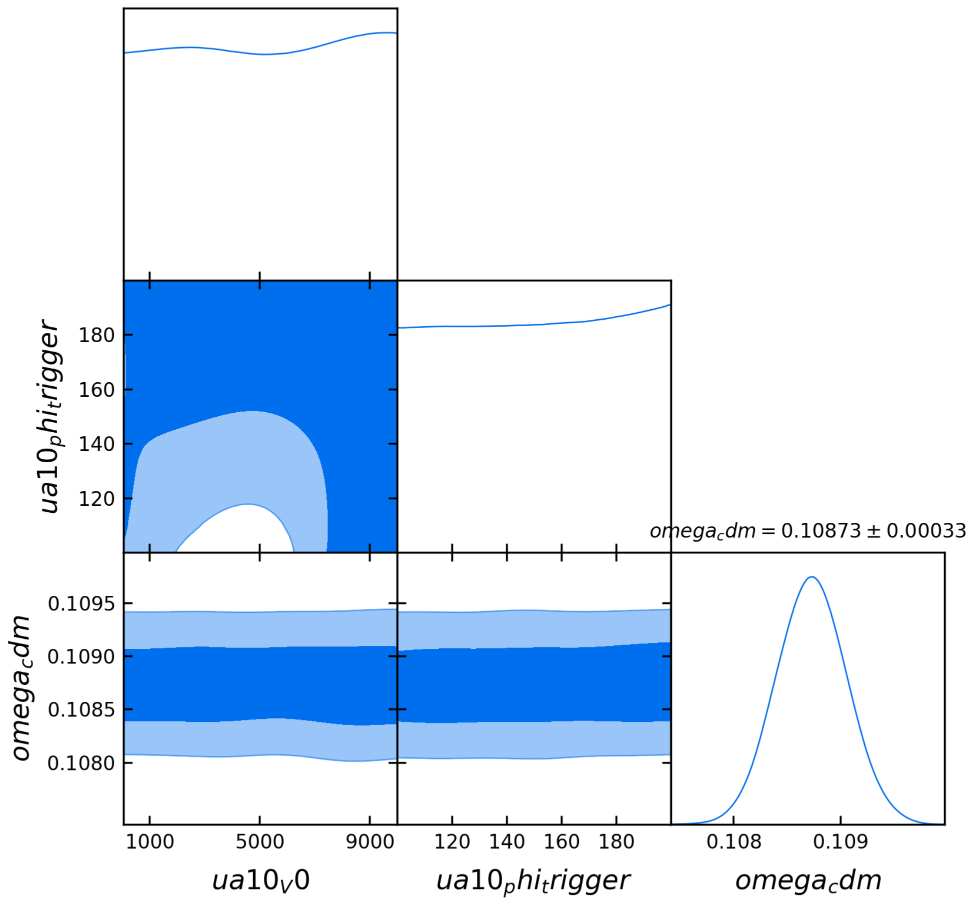

Figure 11: Reported posterior structure for the 137-gated A10 branch. The high-H_0 region is accompanied by a narrow self-adjusted band in $\omega_{\rm cdm}$, indicating that the gated branch behaves as a coupled branch rather than as a one-parameter perturbation.

The model statement is therefore more specific than the vague statement that "137 matters." The integrated chain is narrower and better defined: a spectral sector supplies a localized forcing scale; the Horndeski effective theory produces a downstream stability dome; and the A10 transfer is activated only inside that protected domain, thereby localizing the early-time expansion boost near $z \approx 5000$.

6 Conceptual Support from Root Geometry

The root-geometric component of the program is best treated as a conceptual support for selectivity, not as a literal cosmological derivation. In that construction, an ADE root system with root matrix R defines a bulk Hamiltonian

$$H_\Phi = g\,RR^\top + H_{\text{pert}}, \tag{17}$$

with bulk scale $\lambda_{\max}(H_\Phi) \sim 2gh$ [9, 10]. Observation is restricted to a boundary subspace through

$$P_B = B(B^\dagger B)^{-1}B^\dagger, \tag{18}$$

so that the visible Hamiltonian is $H_{\text{vis}} = P_B H_\Phi P_B$. The visibility of a narrow feature depends not only on the bulk scale but also on suppression of geometric leakage,

$$L(u) := \|QH_\Phi P_B u\|\,, \tag{19}$$

which controls whether the observed mode behaves as an approximate invariant vector of the boundary subspace [11].

The reason to retain this material in the present paper is conceptual. It provides a clean language for selective visibility: a bulk structure may exist, but it becomes sharply visible only when leakage is strongly suppressed by geometric alignment. This is analogous, at the level of mechanism template rather than literal derivation, to the role played by the 137 gate in the cosmological model. The transfer is not merely present; it is selectively activated.

For readability, the supporting numerical diagnostics for the root-geometric sector are collected in Appendix A. The central conclusion drawn from them is limited: selective visibility is highly non-generic under random boundaries and becomes sharp only in a special aligned configuration. That conclusion supports the logic of selectivity, but it is not itself evidence that an ADE eigenvalue is directly measured in cosmological data.

7 Optional Late-Time Extension: Momentum Drag and the S_8 Trade-off

The late-time momentum-drag extension is not part of the foundational A10 trigger. Rather, it addresses a nearby question: whether one can mildly suppress structure growth at late times without immediately violating precision CMB constraints. In the simplest implementation, the cold-dark-matter Euler equation is modified to

$$\dot{\theta}_c + H\theta_c = k^2\psi - \Gamma(a)\theta_c, \tag{20}$$

with

$$\Gamma(a) = \gamma H(a). \tag{21}$$

Mass conservation is preserved while the growth rate of structure is reduced.

The reported outcome is a clear trade-off. Increasing γ lowers S_8 and suppresses the lensing potential, but it also generates oscillatory residuals in the lensed CMB temperature spectrum. The relevant supplementary diagnostics are collected in Appendix B. The resulting interpretation is again deliberately narrow: momentum drag may be a plausible *companion sector* for mild growth suppression, but it is not part of the core mechanism by which the A10 branch raises H_0.

8 Discussion and Scope

The integrated A10 framework is most usefully read as a layered construction with different evidential weights:

1. **Phenomenological early-time branch.** A localized transfer near $z \approx 5000$ can reduce the sound horizon while remaining substantially gentler than a simple constant-$\Delta N_{\rm eff}$ benchmark in TT, with nontrivial but controlled signatures in EE and TE.
2. **Field-space protection.** A spectral-Horndeski sector develops a localized stability dome near $\chi \approx 137$, which supplies a plausible dynamical trigger rather than a hand-imposed injection epoch.
3. **Selective activation.** Root geometry supplies an interpretive template in which sharp visible structure requires leakage suppression. This is not a literal cosmological derivation, but it sharpens the conceptual language of selectivity.
4. **Companion late-time sector.** Momentum drag can modestly lower S_8 only within a constrained window and should therefore be treated as optional rather than foundational.

This hierarchy is important because not every component of the integrated manuscript carries the same evidential status. The most concrete claims are those tied directly to the A10 early-time phenomenology, the CMB/BAO comparisons, and the reported posterior structure of the gated branch. The root-geometric and late-time drag sectors are useful, but they should not be overstated. The paper therefore does *not* claim final model selection over all alternatives, nor does it claim that the number 137 is established as a universal cosmological constant in any stronger sense. What is supported, more narrowly, is that a high-H_0 early-time candidate branch can be organized by a dynamically protected trigger and can remain observationally gentler than several simpler benchmark modifications within the reported tests.

A natural next step is a still more systematic likelihood-based comparison between the gated A10 branch and established benchmark classes across the full CMB, BAO, and large-scale-structure data vector. That is the correct level at which final model selection should be attempted. The present manuscript instead aims to document the internal logic, reported numerical behavior, and sharply delimited scope of the A10 model class.

9 Conclusion

We have presented a claim-bounded diagnostic account of a localized early-time branch within the A10 cosmology program. The core result is a layered candidate branch in which a localized early-time energy-transfer episode near $z \approx 5000$ is organized through a field-space-triggered mechanism associated with a stability window near $\chi \approx 137$. In the reported analyses, this structure yields a high-H_0 candidate branch while leaving the CMB acoustic structure substantially more controlled than a simple constant-$\Delta N_{\rm eff}$ benchmark within the tested setting.

The integrated message is therefore specific and limited. The A10 branch is not merely an arbitrary injection scenario; in its refined form, it combines localization in redshift space, protection in field space, and selective activation in a tightly organized way. The root-geometric analysis gives a useful conceptual model for why selectivity may be non-generic, while the late-time drag sector illustrates how only modest growth suppression appears compatible with small CMB residuals. Taken together, these ingredients point toward a broader methodological lesson: candidate responses to cosmological tensions may benefit from being built as structured mechanisms in which phenomenology, stability, and selectivity are designed together rather than treated as independent afterthoughts. This is a hypothesis-generating and validation-oriented conclusion, not a final model-selection statement.

A Supplementary Root-Geometric Diagnostics

Figure 12 confirms the expected Coxeter scaling of the bulk resonance position. Figure 13 then contrasts random boundaries with an aligned boundary configuration: narrow visibility is highly non-generic unless the observation subspace is arranged so that leakage is strongly suppressed. Figure 14 shows the sensitivity of the leakage measure to boundary perturbations, while Fig. 15 illustrates how spectral shuffling destroys the coherent protection structure.

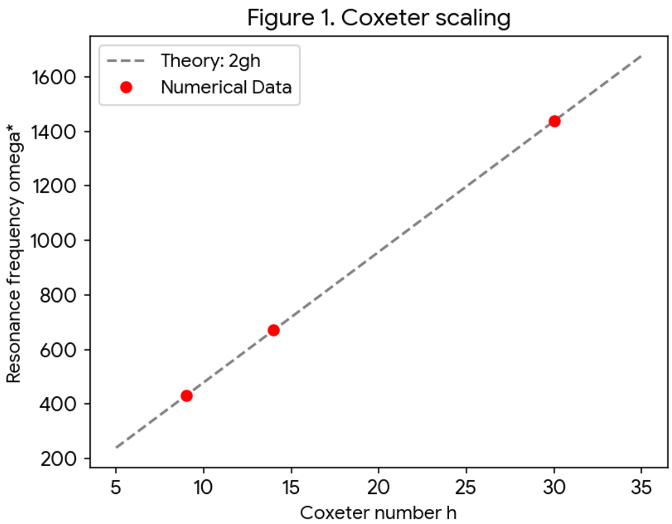

Figure 12: Bulk resonance scale versus Coxeter number in the root-geometric sector. The scaling follows the expected bulk behavior, indicating that the difficulty lies not in bulk scale generation but in conditional visibility.

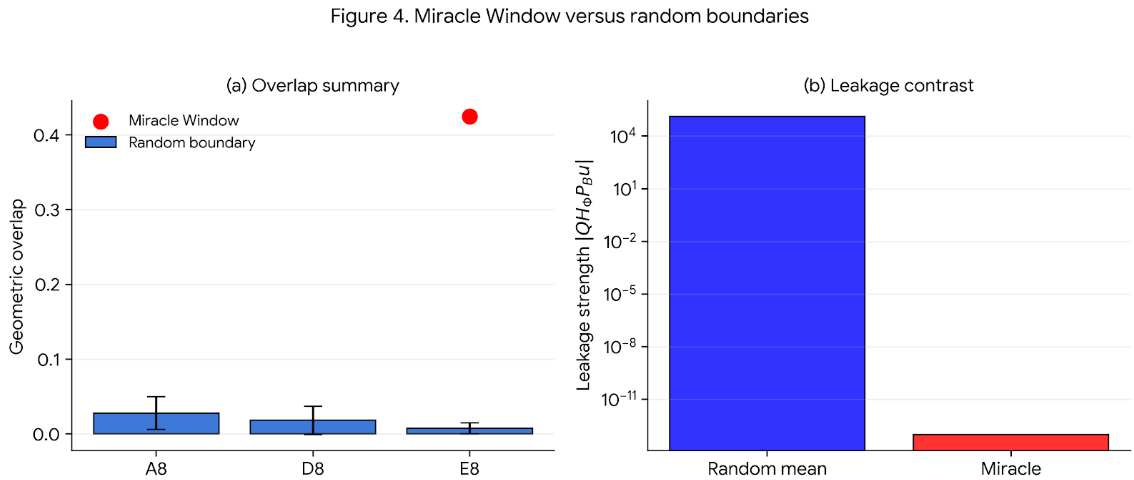

Figure 13: Aligned boundary configuration versus random boundaries. Narrow spectral visibility is highly non-generic under random boundaries and becomes sharp only when leakage into the bulk is strongly suppressed by geometric alignment.

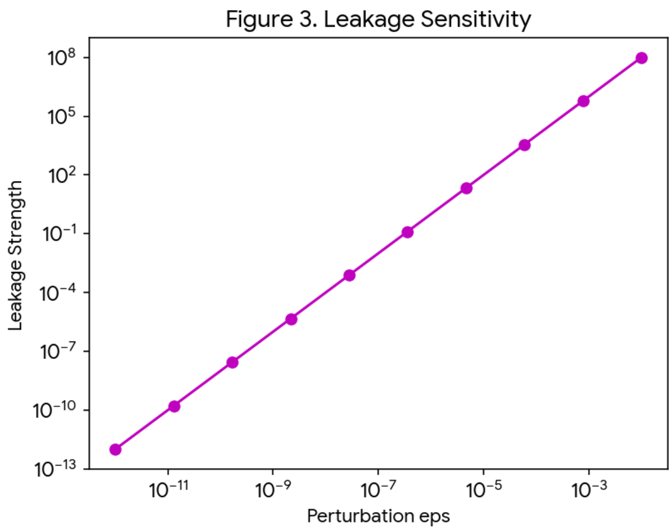

Figure 14: Leakage sensitivity to boundary perturbations. The rapid growth of leakage under perturbation shows that the visible narrow structure is fragile unless the observation subspace remains precisely aligned.

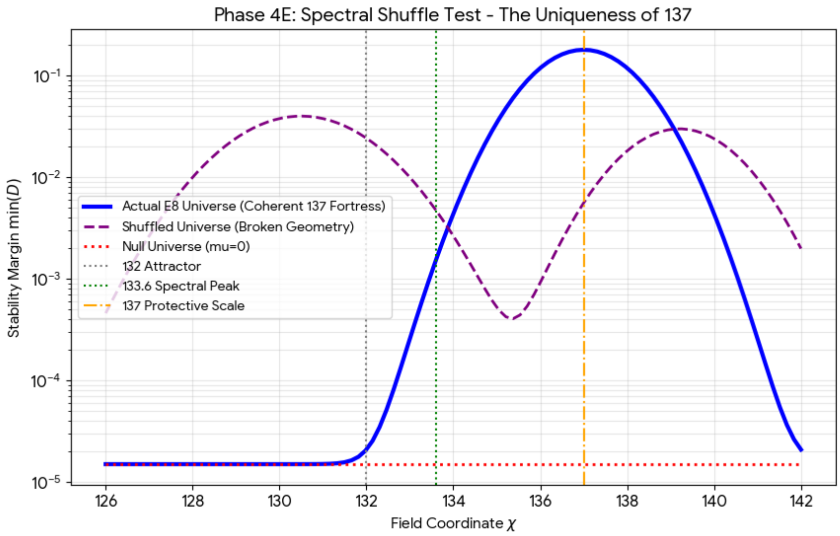

Figure 15: Spectral shuffle diagnostic for the stability structure. Breaking the coherent ordering destroys the localized protection scale, supporting the interpretation that the reported dome is tied to coherent spectral structure rather than to a generic background trend.

B Supplementary Late-Time Drag Diagnostics

The two figures below summarize the narrow viable window for the optional late-time drag sector. Figure 16 shows the joint CMB-temperature and lensing-potential response as the drag strength is increased. Figure 17 shows the corresponding trade-off between S_8 suppression and TT consistency. The message is limited but useful: mild growth suppression is possible, but only at the price of a quickly tightening CMB consistency bound.

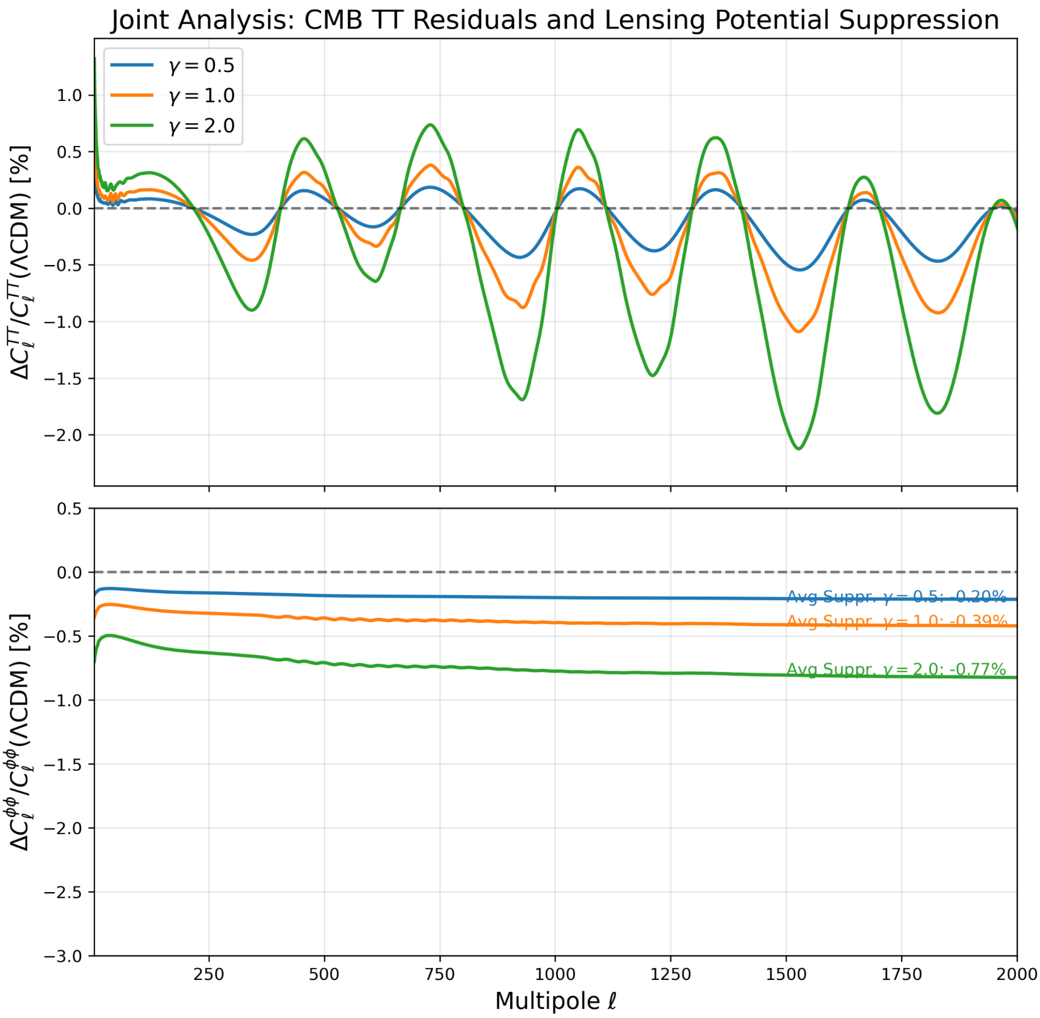

Figure 16: Joint CMB-temperature and lensing-potential residuals in the momentum-drag sector. Increasing drag suppresses the lensing potential but also induces oscillatory TT residuals whose amplitude grows rapidly with γ.

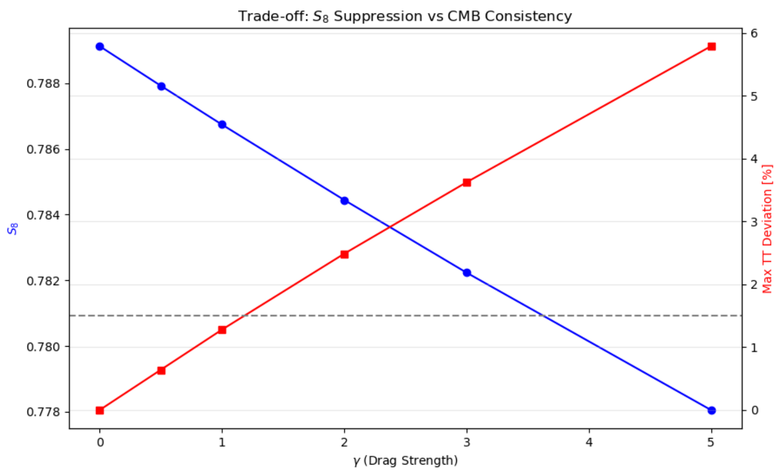

Figure 17: Trade-off between S_8 suppression and TT consistency in the momentum-drag extension. The viable region is confined to modest drag strength, where the reduction in structure growth remains correspondingly modest.

Acknowledgments

The author conceptually designed the study and formulated the core hypotheses. The author acknowledges the use of large language models, including ChatGPT, as computational and editorial assistants for manuscript organization, code-oriented reasoning, and language refinement under the author's direct supervision and validation. The author remains responsible for the final content, claim boundary, and interpretation.

References

[1] Planck Collaboration, N. Aghanim *et al.*, "Planck 2018 results. VI. Cosmological parameters," *Astronomy & Astrophysics* **641**, A6 (2020).

[2] A. G. Riess *et al.*, "A Comprehensive Measurement of the Local Value of the Hubble Constant with $1\,\mathrm{km\,s^{-1}\,Mpc^{-1}}$ Uncertainty from the Hubble Space Telescope and the SH0ES Team," *Astrophysical Journal Letters* **934**, L7 (2022).

[3] T. Karwal and M. Kamionkowski, "Early dark energy, the Hubble-parameter tension, and the string axiverse," *Physical Review D* **94**, 103523 (2016).

[4] V. Poulin, T. L. Smith, T. Karwal, and M. Kamionkowski, "Early Dark Energy Can Resolve the Hubble Tension," *Physical Review Letters* **122**, 221301 (2019).

[5] J. C. Hill, E. McDonough, M. W. Toomey, and S. Alexander, "Early dark energy does not restore cosmological concordance," *Physical Review D* **102**, 043507 (2020).

[6] D. Blas, J. Lesgourgues, and T. Tram, "The Cosmic Linear Anisotropy Solving System (CLASS) II: Approximation schemes," *Journal of Cosmology and Astroparticle Physics* **07**, 034 (2011).

[7] J. Lesgourgues, "The Cosmic Linear Anisotropy Solving System (CLASS) I: Overview," arXiv:1104.2932 [astro-ph.IM] (2011).

[8] S. Alam *et al.*, "The clustering of galaxies in the completed SDSS-III Baryon Oscillation Spectroscopic Survey: cosmological analysis of the DR12 galaxy sample," *Monthly Notices of the Royal Astronomical Society* **470**, 2617–2652 (2017).

[9] J. E. Humphreys, *Reflection Groups and Coxeter Groups* (Cambridge University Press, Cambridge, 1990).

[10] N. Bourbaki, *Lie Groups and Lie Algebras, Chapters 4–6* (Springer, Berlin, 2002).

[11] T. Kato, *Perturbation Theory for Linear Operators* (Springer, Berlin, 1995).